Nat. Hazards Earth Syst. Sci. Discuss., 3, 2883–2912, 2015
www.nat-hazards-earth-syst-sci-discuss.net/3/2883/2015/
doi:10.5194/nhessd-3-2883-2015

Natural Hazards and Earth System Sciences
Open Access
Discussions

Point release wet snow avalanches

C. Vera Valero, Y. Bühler, and P. Bartelt

WSL Institute for Snow and Avalanche Research SLF, Flüelastrasse 11, 7260 Davos Dorf, Switzerland

Received: 17 February 2015 – Accepted: 21 March 2015 – Published: 30 April 2015

Correspondence to: C. Vera Valero (cesar.vera@slf.ch)

Published by Copernicus Publications on behalf of the European Geosciences Union.

Abstract

Wet snow avalanches can initiate from large fracture slabs or small point releases. Point release wet snow avalanches can reach dangerous proportions when they (1) initiate on steep and long avalanche paths and (2) entrain warm moist snow. In this paper we investigate the dynamics of point release wet snow avalanches by applying a numerical model to simulate documented case studies on high altitude slopes in the Chilean Andes (33° S). The model predicts avalanche flow temperature as well as meltwater production, given the thermal initial conditions of the release mass and snowcover entrainment. As the release mass is small, avalanche velocity and runout are primarily controlled by snowcover temperature and moisture content. We demonstrate how the interaction between terrain and entrainment processes influence the production of meltwater and therefore lubrication processes leading to longer runout. This information is useful to avalanche forecasters. An understanding of wet snow avalanche dynamics is important to study how climate change scenarios will influence land usage in mountain regions in the near future.

1 Introduction

The purpose of this paper is to document and discuss the application of numerical avalanche dynamics models to simulate small, point release, wet snow avalanches. The problem is motivated by the increasing frequency of wet snow avalanche events in the central Europe and North America and usually attributed to global warming (Lopez-Moreno et al., 2009; Beniston et al., 2003; McClung, 2013; Pielmeier et al., 2013). Although we have no avalanche statistics to verify this trend, we find ourselves increasingly confronted with the problem of small, wet snow avalanches that disrupt road and railway traffic. This, of course, is a longstanding problem in many mountain regions with maritime climate, e.g. Norway, Alaska, Japan and Chile (Conway and Raymond, 1993; McClung and Schaerer, 2006; McClung and Clarke, 1987; Lackinger, 1987).

NHESSD
3, 2883–2912, 2015

The simulation of wet snow avalanches is not the primary application of existing avalanche dynamics models (Christen et al., 2010; Sampl and Zwinger, 2004; Sheridan et al., 2005; Mergili et al., 2012). Existing models do not consider snow temperature as an initial condition; flow parameters are simply modified to account for the changing mechanical properties of snow with temperature (Voytokskiy, 1977; Bozhinskiy and Losev, 1998). Furthermore point releases either dry or wet have not been simulated before. For example, the Swiss guidelines on avalanche dynamics calculation recommend increasing the velocity dependent turbulent friction to account for the observed lower terminal velocities of wet snow flows (Salm et al., 1990). Experimental field measurements indicate wet snow flows exhibit slower, plug-like velocity profiles where shearing is concentrated at the avalanche base (Dent et al., 1998; Kern et al., 2009), providing some experimental foundation for the suggested increase in turbulent friction. Although it is well-known, that avalanche flow regime is a function of snow cover temperature (see Bozhinskiy and Losev, 1998; Gauer et al., 2008; Issler and Gauer, 2008; Steinkogler et al., 2014), it is only recently that a statistical connection between temperature and avalanche runout has been established (Naaim et al., 2013). The long runout distances of wet avalanches suggest a decrease in Coulomb friction induced by lubricated gliding at the basal boundary, which controls the simulated reach of the avalanche (Buser and Frutiger, 1980).

Snow temperature has been explicitly introduced as a state variable in avalanche dynamics models by Vera et al. (2015). This requires calculating the internal heat energy of the avalanche, which is a function of both, the initial temperature of the snow as well as the avalanche dissipation rate. The temperature of the flowing snow thus varies from initiation to runout (in time) as well as with location in the avalanche (in space). An important assumption of this work is that the heat energy per unit flow area is calculated, but no information can be extracted concerning the distribution of temperature over the flow height. The total heat energy is collapsed down to the basal area. This appears to be satisfactory for the plug-like motion of wet snow flows where shearing is concentrated at the basal layer. A notable result of the model simulations is that the

NHESSD
3, 2883–2912, 2015

entrained snowcover plays an important role in determining the flow temperature of the avalanche. The temperature of the snow in the release zone is important, but the final flow temperature is controlled by the snowcover density and temperature along the track. The density of the entrained snowcover is significant, because it essentially determines the heat energy input by entrainment into the avalanche. For example, a factor two increase in snow density (say from 100 to 200 kg m^{-3}) will change the heat energy content more than a slight change in snow temperature (say from 270 to 272 K).

The model results of Vera et al. (2015) indicate that to simulate wet snow avalanches, accurate information concerning the state of the snowcover is necessary. Snowcover properties determine the onset of meltwater production and therefore the possibility of lubricated gliding. In this paper we simulate four wet snow point release avalanches documented during two winter field campaigns at the high altitude "Cajon del rio Blanco" Valley of the Codelco Andina mine situated 100 km North East from Santiago in the Chilean Andes, well-known for wet snow avalanche activity. To include the important role of snowcover, the field studies are supplemented with SNOWPACK simulations to determine snowpack density and temperature (Bartelt and Lehning, 2002; Lehning et al., 2002). Point release avalanches are modelled using small triangular shaped starting zones, often containing only 100 m^3 of mass. Avalanche growth by entrainment is therefore critical to model the final deposition volume. Avalanche runout, velocity and lateral spreading in complex terrain are reproduced. Forecasting applications are possible in the near future if accurate snow cover information can be coupled with avalanche dynamics calculations to predict extreme avalanche runout.

2 Model

2.1 Model equations

To model avalanche flow in general three-dimensional terrain, we apply depth-averaged model equations for mass, momentum and energy conservation (Christen et al., 2010;

NHESSD
3, 2883–2912, 2015

Vera et al., 2015). The mathematical description of mountain terrain is defined using a horizontal X-Y coordinate system. The elevation $Z(X,Y)$ is specified for each (X,Y) coordinate pair. We introduce a local surface (x,y,z) coordinate system with the directions x and y parallel to the metric geographic coordinates X and Y. The grid of geographic coordinates defines inclined planes with known orientation; the z direction is defined perpendicular to the local x-y plane. Avalanche flow is described by six state variables:

$$\boldsymbol{U}_\Phi = (M_\Phi, M_\Phi u_\Phi, M_\Phi v_\Phi, Rh_\Phi, Eh_\Phi, M_\mathrm{w})^T \quad (1)$$

where M_Φ denote the total mass of the avalanche core (ice and water). The water mass is tracked separately and denoted and M_w. The total mass and water mass is defined per unit flow area. When $M_\mathrm{w} = 0$, the avalanche is termed "dry". The flow height of the total avalanche mass is designated h_Φ. The source of water mass in the snowcover is from rain precipitation, warm temperatures or solar radiation input, etc. This water is defined as an initial condition in the avalanche simulation. Additional water mass can be generated during the avalanche flow by frictional heating. The mass of water always bonded to the moving snow which is moving in the slope parallel direction with velocity $\boldsymbol{u}_\Phi = (u_\Phi, v_\Phi)^T$. Therefore, there is no momentum exchange between the snow ice and liquid phases. Two energy equations are contained in the model formulation: the mechanical free energy R (Bartelt and McArdell, 2009) and the internal heat energy E. These quantities are defined per unit flow volume. The flow temperature of the avalanche T is derived from the internal heat energy E, see Vera et al. (2015).

The model equations can be conveniently written as a vector equation:

$$\frac{\partial \boldsymbol{U}_\Phi}{\partial t} + \frac{\partial \boldsymbol{\Phi}_x}{\partial x} + \frac{\partial \boldsymbol{\Phi}_y}{\partial y} = \boldsymbol{G}_\Phi \quad (2)$$

NHESSD
3, 2883–2912, 2015

where the flux components ($\boldsymbol{\Phi}_x$, $\boldsymbol{\Phi}_y$) are:

$$\boldsymbol{\Phi}_x = \begin{pmatrix} M_\Phi u_\Phi \\ M_\Phi u_\Phi^2 + \frac{1}{2} M_\Phi g' h_\Phi \\ M_\Phi u_\Phi v_\Phi \\ R h_\Phi u_\Phi \\ E h_\Phi u_\Phi \\ M_w u_\Phi \end{pmatrix}, \qquad \boldsymbol{\Phi}_y = \begin{pmatrix} M_\Phi v_\Phi \\ M_\Phi u_\Phi v_\Phi \\ M_\Phi v_\Phi^2 + \frac{1}{2} M_\Phi g' h_\Phi \\ R h_\Phi v_\Phi \\ E h_\Phi v_\Phi \\ M_w v_\Phi \end{pmatrix}. \tag{3}$$

The source terms $\boldsymbol{G}_\Phi$ are

$$\boldsymbol{G}_\Phi = \begin{pmatrix} \dot{Q}_{\Sigma\to\Phi} \\ G_x - S_{\Phi x} - (\dot{Q}_{\Sigma\to\Phi}) u_\Phi \\ G_y - S_{\Phi y} - (\dot{Q}_{\Sigma\to\Phi}) v_\Phi \\ \alpha \dot{W}_\Phi - \beta R h_\Phi \\ (1-\alpha)\dot{W}_\Phi + \beta R h_\Phi + \dot{E}_{\Sigma\to\Phi} h_\Phi - \dot{Q}_w L_f \\ \dot{Q}_w \end{pmatrix}. \tag{4}$$

The flowing avalanche is driven by the gravitational acceleration in the tangential directions $\boldsymbol{G} = (G_x, G_y) = (M_\Phi g_x, M_\Phi g_y)$. The acceleration in the slope perpendicular direction is denoted g' and is composed of gravity g_z and centripetal accelerations f_z (Fischer et al., 2012).

Furthermore the friction and fluidization processes are function of the liquid water content. The snow cover conditions (temperature, density and snow water content) are among the model input parameters and determine the avalanche regime, and run out (Vera et al., 2015).

Frictional resistance is given by the Voellmy-type shear stress (Voellmy, 1955) $\boldsymbol{S}_\Phi = (S_{\Phi x}, S_{\Phi y})^T$, with

$$\boldsymbol{S}_\Phi = \frac{\boldsymbol{u}_\Phi}{\|\boldsymbol{u}_\Phi\|} \left[\mu(R) N + \rho_\Phi g \frac{\|\boldsymbol{u}_\Phi\|^2}{\xi(R)} \right] \tag{5}$$

NHESSD
3, 2883–2912, 2015

that is, the shear stress is a function of the avalanche velocity $\boldsymbol{u}_\Phi$, fluctuation energy R and total normal pressure N in the z direction. The effect of meltwater is to lubricate sliding surfaces, decreasing the dry friction (Colbeck, 1992). We apply the function

$$\mu(h_\mathrm{w}) = \mu_\mathrm{wet} + \left(\mu_0 \exp\left[-\frac{R}{R_0}\right] - \mu_\mathrm{wet}\right) \exp\left[-\frac{h_\mathrm{w}}{h_\mathrm{m}}\right] \tag{6}$$

where μ_wet is the sliding friction coefficient of wet snow ($\mu_\mathrm{wet} = 0.12$) and h_m is a constant defining the decrease of friction as a function of the meltwater content ($h_\mathrm{m} = 0.01$ m). The functional dependency of the friction parameters ξ on R is:

$$\xi(R) = \xi_0 \exp\left(\frac{R}{R_0}\right). \tag{7}$$

2.2 Modeling point release areas

To start an avalanche simulation is necessary to define the initial release volume, V_0. The volume released is calculated by estimating a release area and a mean fracture depth. In case of point released avalanches the released area is reduced to a single dot in the terrain with negligible surface. In this work, point release avalanches are simulated by defining a triangular shaped release area where the upper apex of the triangle is located at the point release. The triangle together with the fracture height defines the initial release volume (see Figs. 4 and 5).

Fracture depth and erosion depths along the avalanche paths were estimated from snow cover and meteorological data. The Codelco Andina mine has automatic weather stations (see Fig. 1) which provide air temperature, snow surface temperature, pressure, wind, precipitation and radiation measurements (see Table 1). The meteorological data was used to run SNOWPACK simulations (Bartelt and Lehning, 2002; Lehning et al., 2002) to define the release temperature and initial snowcover water content. Coupled with the field studies performed by the winter operation crew, provides accurate snow cover information. The distance between the chosen weather station and

NHESSD
3, 2883–2912, 2015

the avalanches paths varies between 0.5 and almost 4.0 km, (see Fig. 1). The release areas in the cases studies were between 3085 and 3600 m a.s.l.; the weather station is located at 3570 m a.s.l. The small elevation distance between the release zones and automatic weather stations ensures accuracy in snow and meteorological data. However, snow surface temperature and surface energy fluxes might be influenced by the slope exposition. SNOWPACK allows the user to generate virtual slopes, specifying slope angle and exposition and coupling the measured meteorological and snow data to the virtual slopes (Bartelt and Lehning, 2002; Lehning et al., 2002). We found no significant differences between the measured data at the weather station location with the calculated values on the virtual slopes. Meteorological data from the winter operation building at the valley bottom (Lagunitas building 2700 m, see Fig. 1) is available. Thus, it was possible to estimate the precipitation and temperature gradients existing between the weather station location and the winter operation building and therefore to estimate the snow cover conditions along the selected avalanche paths.

To estimate the fracture and erosion depths for each case study we considered snow cover temperature and snow water content. The model erodes and releases all the snow cover close to 0 °C and with snow water content higher than 0 mm m^{-2}. This includes moist, wet, very wet and slush snow cover (Fierz et al., 2009) and excludes dry snow cover. The remaining snow input parameters are snow temperature and snow density. These were specified directly using SNOWPACK simulations using the meteorological and snow data collected from the automatic weather station. We compared the simulated snowcover data with field observations to ensure correctness (see Table 1).

The avalanche simulations require the friction (μ_0, ξ_0) and free energy (α, β, R_0) parameters, see Christen et al. (2010) and Bartelt et al. (2012a). The friction parameters were chosen based on the experience simulating wet snow avalanches in the European Alps, Chile and Alaska, Vera et al. (2015). In the four case studies the model parameters remained constant and only slight changes were made in the random kinetic generation α parameter, see Buser and Bartelt (2009). The extremely steep and

NHESSD
3, 2883–2912, 2015

rough gullies fluidized the avalanche and led to higher generation parameters. Simulation parameters for the four case studies are summarized in Table 2.

The equations are solved using the same numerical schemes outlined in Christen et al. (2010).

3 Case studies

We simulated four point release avalanches that occurred in "Cajón del rio Blanco" valley in the Chilean Andes (see Fig. 1). The four cases where spontaneous wet loose point release avalanches that released in periods of high temperature after a recent snowfall (see Table 1). The four avalanches were selected because they reached the primary industrial road in the mine, endangering workers or interrupting mine logistics and communication. The avalanches were subsequently well documented by mine staff (Table 1 and Fig. 8). High resolution digital elevation models (1m) of the terrain are available for the four avalanche tracks. The avalanches are designated Caleta Chica North CCHN-3, Cobalto CG-1, Lagunitas West LGW-2 and Barriga North BN-1.

3.1 Caleta Chica North, CCHN-3

The CCHN-3 is a long, narrow and steep avalanche path that starts at a ridge located at an elevation of 3685 m a.s.l. The path contains a steep gully that includes track segments with steep inclinations of more than 60°. The avalanche path ends directly above the industrial road at 2700 m a.s.l. Although the gully is narrow, the avalanche collects enough snow to endanger the industrial road due to the long distance between the release zone and the deposition area (see Fig. 1).

On the 14 August 2013 between 17:15 and 17:30 LT a point release avalanche released from the top of the avalanche path reaching the industrial road with a final volume of 2000 to 2500 m^3 (estimated by the winter operation crew, see Figs. 8a and 2a). On the 12 August 0.15 m of new snow was recorded at 3500 m a.s.l. A 24 h period

NHESSD
3, 2883–2912, 2015

of cloudy weather followed the snowfall. The 14 August was the first clear sky day after the snow fall from the 12 August. The air temperature at the estimated release time was 3.7 °C at 3550 m a.s.l.

3.2 Cobalto, CG-1

The CG-1 avalanche path is located 2 km to the north (see Fig. 1) of the CCHN-3 with similar west exposition. The track starts at 3465 m a.s.l. and ends at the industrial road at 2450 m a.s.l. The release is located at a steep point located below a ridge. The track is channelized between two vertical rock pillars. The gully between the pillars has an inclination between 60 and 70° for the first 500 vertical meters of drop. The track becomes progressively flatter (about 40–45°) and wider. For the last 300 m elevation drop the gully is between 50 to 70 m wide and the avalanche can entrain large amounts of snow. The deposition area is a open and located on a cone shaped debris fan above the industrial road (see Fig. 1). The surface of the debris fan contains large blocks.

On the 7 September 2013 at 17:30 LT a point release avalanche started from the upper part of the gully, eroding the upper new snow layer. The avalanche reached the valley bottom stopping a few meters above the industrial road (see Figs. 8b and 3a). The volume of the deposits was estimated to be approximately 7000 m^3. On the 6 September a 24 h storm left 0.40 new snow at 3500 m a.s.l. At 2700 m a.s.l., the storm began as a rainfall event, placing 7 mm of water in the snowcover. However, the air temperature dropped at 2700 m and the rain precipitation turned to snow depositing 0.10 m of moist new snow on the wet snowcover. At 2400 m only liquid precipitation was measured. The winter operation crew made two snow profiles at the morning of the 7 August and estimated that the rain reached 2900 m, above this elevation all precipitation fell as snow.

NHESSD
3, 2883–2912, 2015

3.3 Lagunitas West, LGW-2

The LGW-2 avalanche path starts at 3250 m below a rock band and continues over an open slope with 40–45° inclination. The track contains two 5 m drops over rock bands before it gets progressively flatter, reaching a inclination of 30–35°. The track finishes at 2800 m at the industrial road with a 25° inclination (see Fig. 1).

At 14:30 LT on the 9 September 2013 a point avalanche released below the upper rock band reaching the industrial road (see Fig. 4). The 9 September was the first clear sky day after the three day storm and cloudy weather that started on the 6 September. The air temperature at the release time was 8.3 °C.

3.4 Barriga North, BN-1

The BN-1 avalanche path starts directly in front of the winter operation building at 3100 m a.s.l. (see Fig. 1). The release area is south oriented and situated below a wide ridge with 40–45° slope angle. The avalanche path becomes flatter and at the point of maximum steepness the track becomes west exposed, indicating significant channel twist. The avalanche path ends on an industrial road at 2775 m a.s.l., (see Fig. 4).

At 17:30 LT on the 9 September 2013, three hours after the LGW-2 release, a point avalanche released below the wide ridge eroding the new snow. The avalanche passed the channel turn and reached the industrial road (see Fig. 8c). The winter operation crew estimated the avalanche deposits to be approximately 6000 m^3. The air temperature at the released time was 7.8 °C.

The LGW-2 and BN-1 avalanche paths are directly in front of the "Lagunitas" winter operation building (see Fig. 1). The avalanches were observed by mine staff members. Low quality video recordings from mobile phones are available.

NHESSD
3, 2883–2912, 2015

4 Simulation results

In the four case studies the calculated temperature of the flowing snow reached the snow melting temperature and therefore the model predicted the generation of melt water during the flow. The snow cover temperature at the time of release were close to $T \approx 0^{\circ}$. The snowcover was therefore moist (bonded water) or even wet (containing free water), (see Table 1). The calculated avalanches dissipated enough heat energy that the snow within the entire flow was at 0 °C, (see Fig. 10). As meltwater lubricates the avalanche flow, reduced μ values are obtained in the simulations, as the friction parameter μ is function of the water content (Vera et al., 2015). The calculated water content lowered the friction value μ enough to the avalanches reach the valley bottom eroding the existing warm and wet snow cover. With colder and drier snow cover conditions the avalanche simulations show the avalanches would stop immediately after the release.

The set of Figs. 2–5 compares the four run out calculations with the field pictures obtained by the mine winter operation crew. The run out distance were accurately calculated by the model calculations, in the four cases the avalanche run out distances and the deposits extension were correctly estimated. The avalanche flowing height was not possible to measure in any of the four cases. However the final calculations deposits heights (see Figs. 2–5) agree with the rough measurements made by the winter operation crew at the field (see Fig. 8).

Figure 7 shows the increase in avalanche volume over time from the initial release $t = 0$ until deposition for the four case studies. The calculations are normalized with the initial release volumes. The final calculated volumes reach values between twenty and sixty times the initial release volume. The calculations also reveal that in the examples CG-1 and CCHN-3 the avalanche simulations did not entrained more snow after the avalanche reached the track midpoint. In these two examples there was no snow cover below 2900 m (see Figs. 2 and 3) and therefore the final ratio between the final deposit volume and the initial volume are the lowest, (between 20 and 30 times

NHESSD
3, 2883–2912, 2015

the initial release volume). Figure 9 depicts the avalanche volume with the avalanche time for the 4 cases studies. At $t = 0$ the plot shows the initial release mass. For the examples CG-1 and CCHN-3 the volume increase flattens at the point the avalanche is no longer eroding snow. The final calculated deposition volumes are in agreement with the observations made by the winter operation crew.

The Fig. 6 indicates maximum velocity calculations in the LGW-2 and BN-1 case studies. Avalanches velocity could be roughly estimated through mobile phone video recordings. The estimated velocity measurements coincide with the velocity calculations made by the model (about $10\,\mathrm{m\,s^{-1}}$). Unfortunately the approximation techniques are not accurate enough to perform a more precise analysis.

5 Discussion

The results presented in this paper are valid for mountain rock faces with well defined flow channels and also open slopes. At release the avalanche mass spreads depending on the terrain features. In two of the four case studies, avalanche spreading was inhibited by the steep sidewalls of mountain gullies, a function of the topographic properties of the mountain. The other two examples where open slopes where the spreading angle was larger than in the channelized cases but controlled too by topographic features. Avalanche movement is therefore not only controlled by the thermal state of the snow, but also by the slope geometry. High resolution digital elevation models that accurately represent mountain ravines and channels are thus necessary to apply avalanche dynamics models to simulate small avalanches (Bühler et al., 2011). In open terrain (BN-1, LGW-2), the lateral spreading of the avalanche is modeled.

The position of all release zones was obtained from the eyewitness reports and post-event surveys. Entrainment depths for the simulations were also obtained from field studies and event documentation. From automated weather stations good estimates of snow temperature could be obtained. Because the avalanches disrupted road traffic, road clearance crews could estimate deposition depths allowing good estimates of

NHESSD
3, 2883–2912, 2015

avalanche mass balance. The velocity measurements are not accurate enough to assess the model performance. Nevertheless the data available showed that the model's velocity output is accurate in first approximation.

The model calculated the snow temperature from initiation to runout. Due to the warm initial conditions the investigated avalanches reached the melting point of snow-ice almost immediately after release. The entrainment of warm, moist snow enhanced the lubrication process. The decrease of Coulomb friction due to lubrication effects is key for small point release avalanches to develop into long-running wet snow avalanches. For practical applications it is important that lubrication processes due to the (1) initial snow water content, (2) snow melting by frictional dissipation and (3) heat energy of entrained snow must all be taken into account. The model includes a lubrication relationship between meltwater content and the Coulomb friction parameter μ. The lubrication model is an empirical necessity that needs to be improved with additional mechanical tests.

To back-calculate the four case studies the same set of model parameters used previously in Vera et al. (2015) was applied. The model results emphasize that complete information of the snow cover is necessary to achieve accurate representations of the events. The model is sensible to variations in the initial snow cover conditions (temperature and water content). For example, when colder snow is specified at release, the avalanche simulations stop immediately after the release without reaching the valley bottom. However given accurate initial conditions the model was able to back calculate accurately runout distances, avalanche outline and avalanche volumes in the four case studies. It is therefore only possible to obtain realistic runout predictions with accurate snow cover data. The application of the avalanche dynamics model should be restricted to cases where accurate data is available.

The method used to simulate the avalanche point release requires defining a small triangular area. The ratio between the eroded snow volume and the initial snow volume is between 20 to 60 for the four case studies we studied in this paper. The initial area

NHESSD
3, 2883–2912, 2015

used to simulate the avalanche release does not affect the final run-out, velocity and avalanche deposit calculations.

6 Conclusions

Avalanche dynamics models have been traditionally applied to simulate large, dry, slab release avalanches. The starting volumes of such avalanches are typically larger than $V_0 > 50\,000\,m^3$. The primary application is to prepare avalanche hazard maps which are based on extreme events with long return periods. In this work we applied a snow avalanche model to simulate small, wet, point release avalanches. Avalanche release mass was modeled using small triangular shaped release zones containing less than $V_0 \approx 100\,m^3$ of snow. The purpose of the simulations was to help avalanche warning experts determine whether a logistically important road should remain open or be closed. The application of an avalanche dynamics model to simulate small, point release avalanches is novel and poses many new challenges. Three preconditions for the simulation of such small avalanche events are:

1. The availability of high resolution digital terrain models
2. Simulation of snow entrainment to model avalanche growth
3. Reliable snowcover information, including snow temperature

Finally, this work demonstrates that not only large, wet snow slab avalanches can develop significant destructive power. Wet snow point avalanches releasing from steep slopes and long avalanche paths collect enough snow to disrupt and harm human activities. The application of an avalanche dynamics model was tested for two winter seasons in the Andina mine (Chile). After initial promising results, the operational application of an avalanche dynamics model is planned. Simulations coupled with accurate and continually updated snow cover and meteorological information is required to predict avalanche run outs and deposition volumes. The model does not provide

NHESSD
3, 2883–2912, 2015

any indication whether the avalanche is going to release or not, but if the avalanche releases the model gives a good indication of the potential run out distances and deposition volumes.

Acknowledgements. Financial support for this project was provided by Codelco Mining, Andina Division (Chile). The authors thank A. Ellena and L. Cornejo for starting the project and their helpful insights into the wet snow avalanche problem. In addition we thank all avalanche alert center members: L. Gallardo, M. Didier and P. Cerda, not only for their support, but also for their confidence, patience and enormous help during the last three winters in the Andina mine.

References

Bartelt, P. and Lehning, M.: A physical SNOWPACK model for the Swiss avalanche warning, Part I: Numerical model, Cold Reg. Sci. Technol., 35, 123–145, doi:10.1016/S0165-232X(02)00074-5, 2002. 2886, 2889, 2890, 2901

Bartelt, P. and McArdell, B.: Granulometric investigations of snow avalanches, J. Glaciol., 55, 829–833, 2009. 2887

Bartelt, P., Bühler, Y., Buser, O., Christen, M., and Meier, L.: Modeling mass-dependent flow regime transitions to predict the stopping and depositional behaviour of snow avalanches, J. Geophys. Res., 117, F01015, doi:10.1029/2010JF001957, 2012. 2890

Beniston, M., Keller, F., Koffi, B., and Goyette, S.: Estimates of snow accumulation and volume in the Swiss Alps under changing climatic conditions, Theor. Appl. Climatol., 76, 125–140, doi:10.1007/s00704-003-0016-5, 2003. 2884

Bozhinskiy, A. N. and Losev, K. S.: The Fundamentals of Avalanche Science, Mitt. Eidgenöss. Inst. Schnee-Lawinenforsch., Davos, 280 pp., 1998. 2885

Bühler, Y., Christen, M., Kowalsky, J., and Bartelt, P.: Sensitivity of snow avalanche simulations to digital elevation model quality and resolution, Ann. Glaciol., 52, 72–80, 2011. 2895

Buser, O. and Bartelt, P.: Production and decay of random kinetic energy in granular snow avalanches, J. Glaciol., 55, 3–12, 2009. 2890

Buser, O. and Frutiger, H.: Observed maximum run-out distance of snow avalanches and determination of the friction coefficients, J. Glaciol., 26, 121–130, 1980. 2885

NHESSD

3, 2883–2912, 2015

Christen, M., Kowalski, J., and Bartelt, P.: RAMMS: numerical simulation of dense snow avalanches in three-dimensional terrain, Cold Reg. Sci. Technol., 63(2010), 2–14, doi:10.1016/j.coldregions.2010.04.005, 2010. 2885, 2886, 2890, 2891

Colbeck, S.: A Review of the Processes that Control Snow Friction, Cold Regions Research and Engineering Lab, 92-2, 1992. 2889

Conway, H. and Raymond, C.: Snow stability during rain, J. Glaciol., 39, 635–642, 1993. 2884

Dent, J. D., Burrell, K., J., Schmidt, D. S., Louge, M. Y., Adams, E. E., and Jazbutis, T. G.: Density, velocity and friction measurements in a dry snow avalanche, Ann. Glaciol., 26, 247–252, 1998. 2885

Fierz, C., Armstrong, R., Durand, Y., Etchevers, P., Greene, E., McClung, D., Nishimura, K., Satyawali, P., and Sokratov, S.: The International Classification for Seasonal Snow on the Ground (ICSSG) IHP-VII Technical Documents in Hydrology, No. 83, IACS Contribution No. 1, UNESCO-IHP, 2009. 2890

Fischer, J., Kowalski, J., and Pudasaini, S.: Topographic curvature effects in applied avalanche modeling, Cold Reg. Sci. Technol., 74–75, 21–30, doi:10.1016/j.coldregions.2012.01.005, 2012. 2888

Gauer, P., Issler, D., Lied, K., Kristensen, K., and Sandersen, F.: On snow avalanche flow regimes: inferences from observations and measurements, Proceedings of the International Snow Science Workshop, ISSW 2008, 21–27 September, Whistler, Canada, 2008. 2885

Issler, D. and Gauer, P.: Exploring the significance of the fluidised flow regime for avalanche hazard mapping, Ann. Glaciol., 49, 193–198, 2008. 2885

Kern, M., Bartelt, P., Sovilla, B., and Buser, O.: Measured shear rates in large dry and wet snow avalanches, J. Glaciol., 55, 327–338, 2009. 2885

Lackinger, B.: Stability and fracture of the snow pack for glide avalanches, in: Avalanche Formation, Movement and Effects Symposium at Davos 1986, edited by: Salm, B. and Gubler, H., IAHS Publ., 162, Davos, 229–240, 1987. 2884

Lehning, M., Bartelt, P., Brown, B., Fierz, C., and Satyawali, P.: A physical SNOWPACK model for the Swiss avalanche warning, Part II: Snow microstructure, Cold Reg. Sci. Technol., 35, 147–167, doi:10.1016/S0165-232X(02)00073-3, 2002. 2886, 2889, 2890, 2901

Lopez-Moreno, J. L., Goyetteb, S., and Benistonb, M.: Impact of climate change on snowpack in the Pyrenees: horizontal spatial variability and vertical gradients, J. Hydrol., 374, 384–396, doi:10.1016/j.jhydrol.2009.06.049, 2009. 2884

NHESSD

3, 2883–2912, 2015

McClung, D.: The effects of El Niño and La Niña on snow and avalanche patterns in British Columbia, Canada, and central Chile, J. Glaciol., 59, 783–792, 2013. 2884
McClung, D. and Clarke, G. K. C.: The effects of free water on snow gliding, J. Geophys. Res., 92, 6301–6309, 1987. 2884
McClung, D. and Schaerer, P.: The Avalanche Handbook, 3rd Edn., Mountaineers Books, 1615 Venables St, Vancouver, B.C. Canada, 2006. 2884
Mergili, M., Schratz, K., Ostermann, A., and Fellin, W.: Physically-based modelling of granular flows with Open Source GIS, Nat. Hazards Earth Syst. Sci., 12, 187–200, doi:10.5194/nhess-12-187-2012, 2012. 2885
Naaim, M., Durand, Y., Eckert, N., and Chambon, G.: Dense avalanche friction coefficients: influence of physical properties of snow, J. Glaciol., 59, 771–782, 2013. 2885
Pielmeier, C., Techel, F., Marty, C., and Stucki, T.: Wet snow avalanche activity in the Swiss Alps – trend analysis for mid-winter season, International Snow Science Workshop 2013, Proceedings, ISSW 2013, 7–11 October 2013, Grenoble – Chamonix Mont Blanc, 253–258, 2013. 2884
Steinkogler, W., Sovilla, B., and Lehning, M.: Influence of snow cover properties on avalanche dynamics, Cold Reg. Sci. Technol., 97, 121–131, 2014. 2885
Salm, B., Burkard, A., and Gubler, H.: Berechnung von Fliesslawinen: eine Anleitung fuer Praktiker mit Beispielen, Eidg. Inst. Schnee- und Lawinenforschung, Mitteilung 47, Ann. Glaciol., 18, 221–226, 1990. 2885
Sampl, P. and Zwinger, T.: Avalanche simulation with SAMOS, Ann. Glaciol., 38, 393–398, 2004. 2885
Sheridan, M., Stinton, A., Patra, A., Pitman, E., Bauer, A., and Nichita, C.: Evaluating Titan2D mass-flow model using the 1963 Little Tahoma Peak avalanches, Mount Rainier, Washington, J. Volcanol. Geoth. Res., 139, 89–102, 2005. 2885
Vera, C., Bühler, Y., Wikstroem Jones, K., and Bartelt, P.: Release temperature, snowcover entrainment and the thermal flow regime of snow avalanches, J. Glaciol., 61, 173–184, 2015. 2885, 2886, 2887, 2888, 2890, 2894, 2896
Voellmy, A.: Ueber die Zerstoerungskraft von Lawinen, Schweiz. Bauztg., 73, 280–285; 159–162; 212–217; 246–249; 280–285, 1955. 2888
Voytkovskiy, K. F.: Mekhanicheskiye svoystva snega, Mechanical properties of snow, translated by: Bartelt, C. E., Sibirskoye Otdeleniye, Institut Merzlotovedeniya, Nauka, Moscow, 1977. 2885

NHESSD
3, 2883–2912, 2015

Table 1. Summary of the snow and meteorological conditions in the four cases studies at the estimated release time. Note the first data section corresponds to direct measurements from the automatic weather station (AT, New Snow, SST and $\Delta SST_{12\,h}$). The second section contains simulated data from SNOWPACK calculations (Bartelt and Lehning, 2002; Lehning et al., 2002).

Parameter	BN-1 Simulation	LGW-2 Simulation	CG-1 Simulations	CCHN-3 Simulation
Air temperature AT (°C)	7.8	8.3	−3.0	3.7
New $snow_{72\,h}$ (m)	0.28	0.28	0.4	0
Snow surface temperature SST (°C)	−0.2	−0.08	−1.1	−2.1
$\Delta SST_{12\,h}$ (°C)*	9.2	5.2	11.8	16.17
Snow release temperature (°C)	−0.9	−0.9	−0.5	−0.8
Net energy $flux_{12\,h}$ (W m^{-2})	73.55	71.55	79.95	324.22
Snow water content SWC (mm m^{-2})	0.9	0.85	1.07	0.12
Snow density (kg m^{-3})	240	235	185	190

* $\Delta SST_{12\,h}$ is the change in snow surface temperature in the last 12 h before the avalanche released.

NHESSD
3, 2883–2912, 2015

Table 2. Summary of input and simulation parameters for the four calculations examples.

Parameter*	BN-1 Simulation	LGW-2 Simulation	CG-1 Simulation	CCHN-3 Simulation
Grid size	2 m	2 m	2 m	2 m
μ	0.55	0.55	0.55	0.55
Cohesion C	50 Pa	50 Pa	60 Pa	60 Pa
ξ	1300 m s^{-2}	1300 m s^{-2}	1300 m s^{-2}	1300 m s^{-2}
α	0.07	0.08	0.08	0.08
β	1.0	1.0	1.0	1.0
V_0	248 m^3	326 m^3	679 m^3	130 m^3
h_0	0.40 m	0.30 m	0.40 m	0.30 m
Snow Water content (SWC$_0$)	0.95 mm m^{-1}	0.85 mm m^{-1}	1 mm m^{-1}	0 mm m^{-1}
ρ_Σ	240 kg m^{-3}	235 kg m^{-3}	300 kg m^{-3}	250 kg m^{-3}
h_Σ	0.40 – Δ0.05 m	0.30 – Δ0.05 m	0.40 – Δ0.07 m	0.30 – Δ0.05 m
T_0	0 °C	0 °C	0 °C	0 °C
T_Σ	0 °C	0 °C	0 °C	0 °C
Snow Water content (SWC$_\Sigma$)	1 mm m^{-2}	1 mm m^{-2}	1 mm m^{-2}	0.5 mm m^{-2}
Ratio (Final volume/Release volume)	64	45	20	28

* Parameters with the sub index "0" denote fields related with the release mass. Parameters with the sub index "Σ" denote fields related with the eroded mass. h_Σ denotes the amount of eroded snow, the first quantity shows the eroded mass at the altitude of the release. The quantity coming with Δ shows the decrease of eroded mass per 100 m of altitude. h_0 denotes the fracture height at the released.

NHESSD
3, 2883–2912, 2015

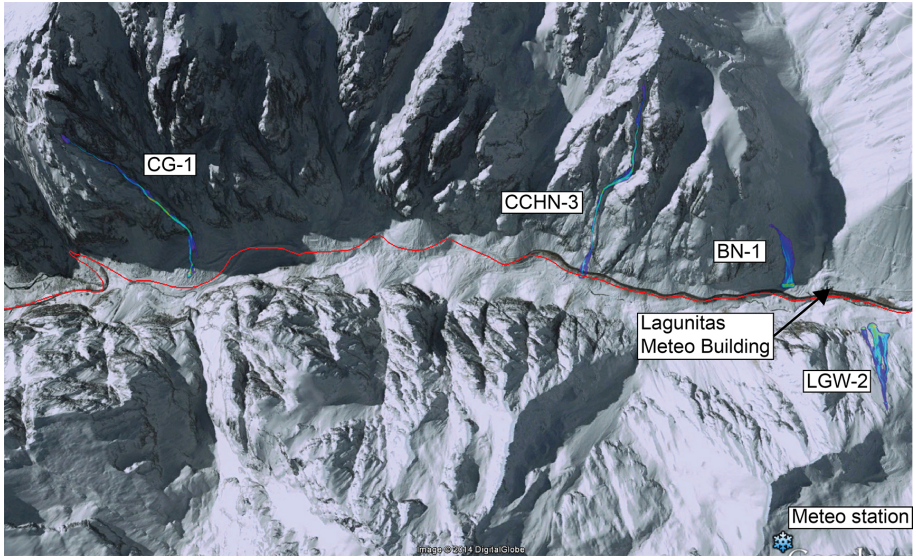

Figure 1. Location overview from the four avalanche simulations. The red line notes the main industrial road. The snow flake on the bottom right corner indicates the exact position from the automatic weather station. "Lagunitas" meteo building is located at valley bottom at 2700 m a.s.l. Image captured from Google Earth.

NHESSD
3, 2883–2912, 2015

Figure 2. Avalanche deposits: **(a)** CCHN-3, **(b)** CG-1 and **(c)** BN-1. The outline, height and volume of the deposits was measured by the winter operation crew immediately after the industrial road was open.

NHESSD
3, 2883–2912, 2015

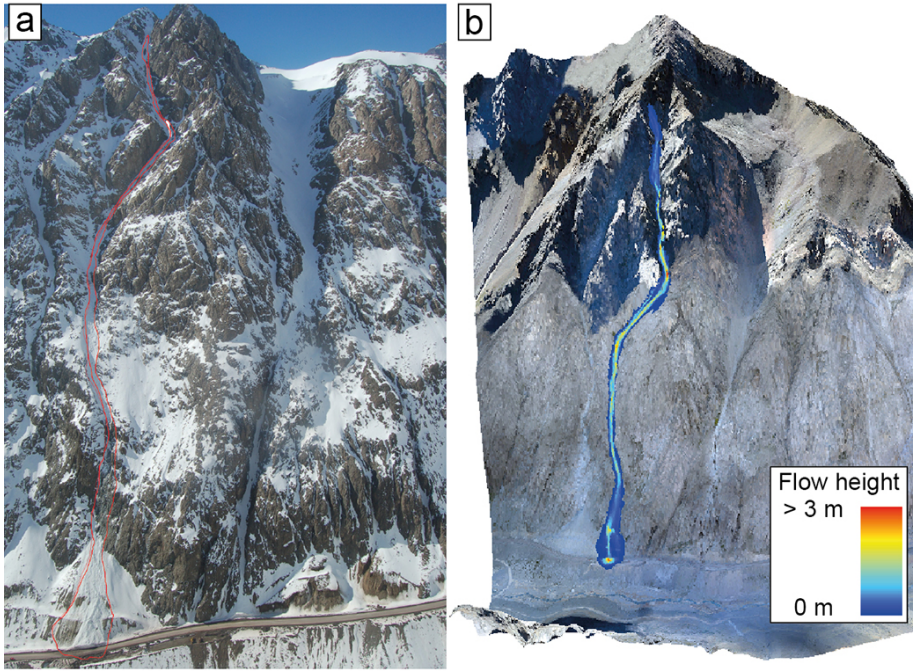

Figure 3. (a) CCHN-3 avalanche picture taken from the helicopter the day after the release. The point release was on the top the steep gully on a rock face. The avalanche crossed the industrial road (see Fig. 8a). **(b)** Maximum flow height simulation. The model estimated correctly the run out distance and the avalanche deposits.

NHESSD
3, 2883–2912, 2015

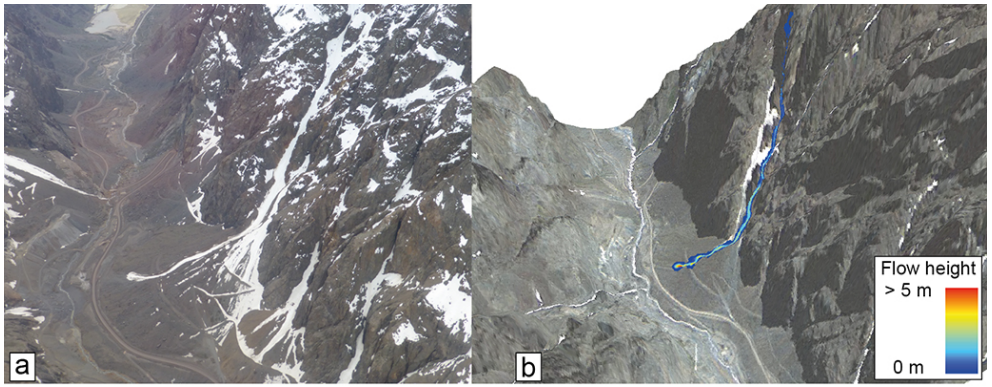

Figure 4. (a) Avalanche path CG-1. Image taken from the helicopter the day after the release. The avalanche stopped eroding snow at 2900 m a.s.l. but kept flowing till reaching the valley bottom over a gravel surface. **(b)** Maximum flow height simulation. The model estimated correctly the run out distance and avalanche outline and volume.

NHESSD
3, 2883–2912, 2015

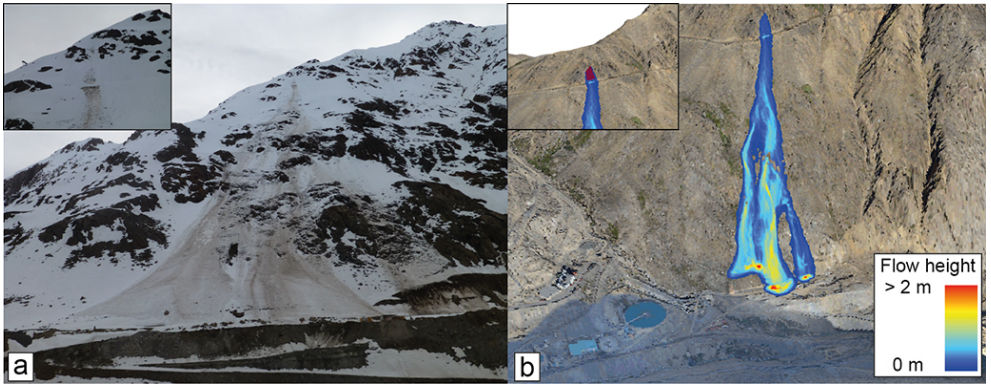

Figure 5. (a) Avalanche LGW-2 picture taken from the valley bottom. The avalanche released below a rock band and spread over the slope flowing over two rock bands before reaching a secondary road at the valley bottom. Top left shows a closer view from the release point. **(b)** Flow height simulation. The model calculated correctly the three avalanche arms getting an accurate avalanche outline simulation. Avalanche run-out distance, avalanche outline and avalanche spreading angle were correctly calculated by the model. On the top left a closer view with the calculated release area (in red) is shown.

NHESSD
3, 2883–2912, 2015

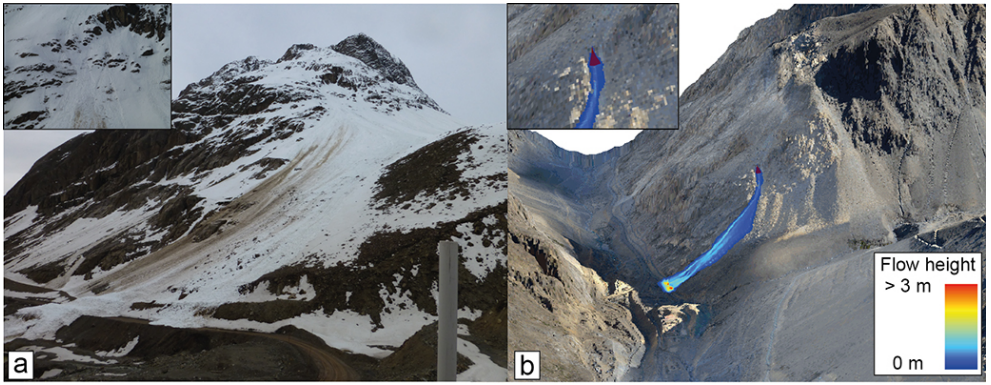

Figure 6. (a) Picture from the BN-1 avalanche taken from the "Lagunitas" meteo building some minutes after it happened. The avalanche crossed a secondary industrial road reaching the avalanche deposits 4 m of snow at the road (see Fig. 2c). On the top left closer view from the point release. **(b)** Flow height simulations from the BN-1 avalanche. The model calculated accurately the avalanche run out distance, the avalanche outline including the curve done by the avalanche on half way from the avalanche path and the avalanche spreading angle. On the top left the calculated released area (in red) is shown.

NHESSD
3, 2883–2912, 2015

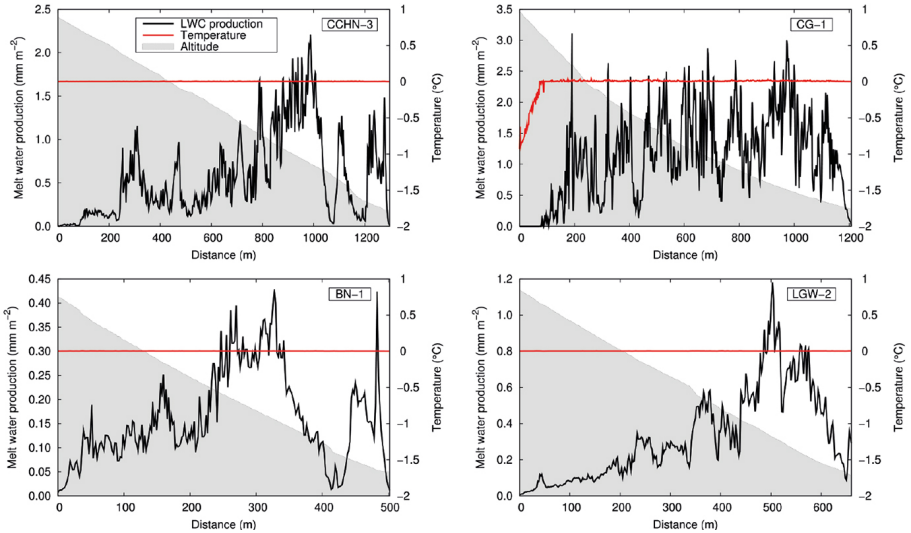

Figure 7. Temperature and melt water production calculations for the four case studies. The avalanches temperature keep close to 0 °C or constant equals zero during the whole avalanche simulation. Release temperatures and entrainment temperatures were close to zero in the four case studies, therefore the model immediately started melting snow into water. The model calculated from 0.5 till 3 mm m^{-2} of melt water production in the four case studies.

NHESSD
3, 2883–2912, 2015

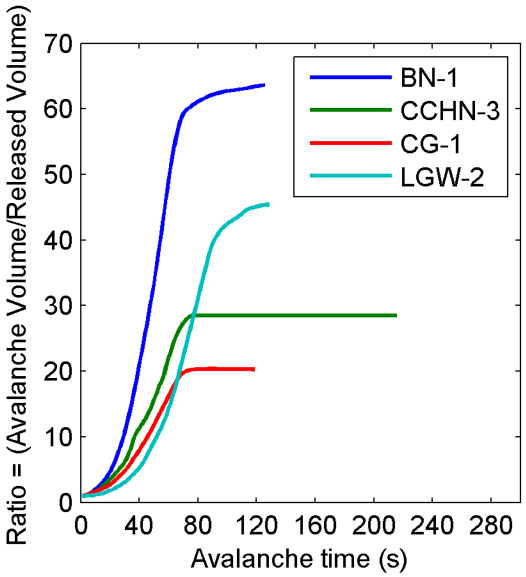

Figure 8. Ratio between the avalanche flowing volume and the initial release volume. The *x* axis show the avalanche time since the release till the last mass unit stopped. In the four case studies the ratio between the final volume and the initial released volume is between 20 and 60 times.

NHESSD
3, 2883–2912, 2015

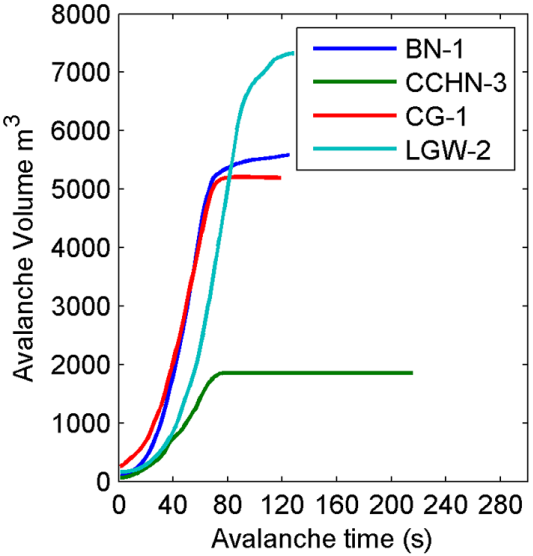

Figure 9. Avalanche volume calculations for the four case studies. The *x* axis show the avalanche time since the release till the last unit of mass stopped. Flat curves show time when the avalanches were not entrainning additional snow, (cases CG-1 and CCHN-3).

NHESSD
3, 2883–2912, 2015

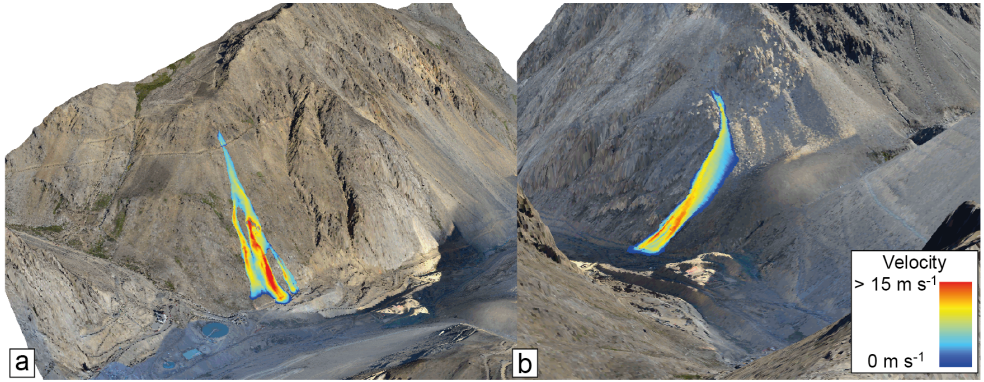

Figure 10. Calculated maximum velocities of the LGW-2 avalanche **(a)** and of the BN-1 avalanche **(b)**.

NHESSD
3, 2883–2912, 2015